

Improving Precipitation Forecasts with Convolutional Neural Networks

Anirudhan Badrinath¹, Luca Delle Monache², Negin Hayatbini³, William Eric Chapman⁴, Forest Cannon⁴, and F. Martin Ralph⁵

¹University of California, Berkeley

²University of California San Diego

³Center for Western Weather and Water Extremes, Scripps Institution of Oceanography

⁴University of California, San Diego

⁵SIO

November 21, 2022

Abstract

Traditional post-processing methods have relied on point-based applications that are unable to capture complex spatial precipitation error patterns. With novel ML methods using convolution to more effectively identify and reduce spatial biases, we propose a modified U-Net convolutional neural network (CNN) to post-process daily accumulated precipitation over the US west coast. For training, we leverage 34 years of deterministic Western Weather Research and Forecasting (West-WRF) reforecasts. On an unseen 4-year data set, the trained CNN yields a 12.9-15.9% reduction in root mean-square error (RMSE) over West-WRF for lead times of 1-4 days. Compared to an adapted Model Output Statistics baseline, the CNN reduced RMSE by 7.4-8.9% for all events. Effectively, the CNN adds more than a day of predictive skill when compared to West-WRF. The CNN outperforms the other methods also for the prediction of extreme events, highlighting a promising path forward for improving precipitation forecasts.

Improving Precipitation Forecasts with Convolutional Neural Networks

Anirudhan Badrinath¹, Luca Delle Monache², Negin Hayatbini², Will
Chapman², Forest Cannon², Marty Ralph²

¹Department of Computer Science, University of California Berkeley, Berkeley, California, United States

²Center for Western Weather and Water Extremes, Scripps Institution of Oceanography, University of
California San Diego, La Jolla, California, United States

Key Points:

- We adapted a U-Net convolutional neural network (CNN) architecture as a post-processing framework.
- The precipitation class imbalance was addressed by the dual ML model approach.
- The proposed method provides greater numerical accuracy over all lead times.

Corresponding author: Anirudhan Badrinath, abadrinath@berkeley.edu

Abstract

Traditional post-processing methods have relied on point-based applications that are unable to capture complex spatial precipitation error patterns. With novel ML methods using convolution to more effectively identify and reduce spatial biases, we propose a modified U-Net convolutional neural network (CNN) to post-process daily accumulated precipitation over the US west coast. For training, we leverage 34 years of deterministic Western Weather Research and Forecasting (West-WRF) reforecasts.

On an unseen 4-year data set, the trained CNN yields a 12.9-15.9% reduction in root mean-square error (RMSE) over West-WRF for lead times of 1-4 days. Compared to an adapted Model Output Statistics baseline, the CNN reduced RMSE by 7.4-8.9% for all events. Effectively, the CNN adds more than a day of predictive skill when compared to West-WRF. The CNN outperforms the other methods also for the prediction of extreme events, highlighting a promising path forward for improving precipitation forecasts.

Plain Language Summary

Machine learning methods are used for accurate large-scale prediction by learning patterns from a vast amount of data. We demonstrate the utility of a computer vision-based machine learning technique for improving precipitation forecasts. Extreme precipitation events and atmospheric rivers, which contain narrow bands of water vapor transport, can cause millions in damages. We show that there is a significant increase in predictive accuracy for daily accumulated precipitation using these machine learning methods, which could result in significant societal benefits.

1 Introduction

The precipitation associated with atmospheric rivers (ARs), "a long, narrow, and transient corridor of strong horizontal water vapor transport" (AMS, 2019), replenishes the water supply but can also result in flooding over the western United States. ARs cause median economic losses in the tens to hundreds of millions of dollars for AR4 and AR5 ARs based on the AR scale developed by (Ralph et al., 2019). Further, ARs have been identified as the primary source of hydrologic flooding in the western United States (Corringham et al., 2019). Accurate and reliable predictions of precipitation can help in minimizing losses attributable to ARs or other weather phenomena (e.g., cut-off lows, narrow cold-frontal rainbands, etc.) and in better managing the water supply in the western United States (ODonnell et al., 2020).

Numerical weather prediction (NWP) are based on dynamical models that are built on current state-of-the-science knowledge of key atmospheric physics and numerical procedure. However, NWP accuracy is affected by initial condition errors, numerical approximations, and incomplete understanding and representation of all the relevant physical processes (Delle Monache et al., 2013; Vannitsem & Ghil, 2017; Collins & Allen, 2002; Nicolis & Nicolis, 2007).

NWP post-processing methods are designed to correct for the aforementioned deficiencies by learning the characteristics of NWP errors from a historical data set to then try to anticipate today forecast biases. These include downscaling methods, Kalman filters, model output statistics (MOS), and machine learning methods such as neural network models, decision trees, and multilinear regression models (Louka et al., 2008; Glahn & Lowry, 1972). Historically, post-processing methods, including machine learning methods, have operated on a point-by-point basis (Rasp & Lerch, 2018). Recently, convolutional neural networks (CNNs) have been proposed to correct satellite retrievals (Tao et al., 2016). CNNs have been shown to be a powerful regression tool in the domains of

61 image analysis (Krizhevsky et al., 2012). For NWP, recent work by W. Chapman et al.
62 (2019) has highlighted the efficacy of a CNN as a NWP post-processing method for the
63 prediction of integrated vapor transport (IVT). It was shown that the CNN-based pre-
64 diction resulted in 9-17% improvements in RMSE as compared to other methods (W. Chap-
65 man et al., 2019).

66 Traditional point-by-point approaches have been shown to be effective in improv-
67 ing the raw estimates of dynamical models (Glahn & Lowry, 1972), and are particularly
68 valuable for certain applications, e.g., renewable energy (Alessandrini et al., 2015; Cer-
69 vone et al., 2017). However, since spatial interdependence is ignored, at times non-physical
70 fields with statistical anomalies are produced (Vannitsem & Ghil, 2017). Further, the
71 predominantly “no rain” data points in the precipitation field poses an issue for stan-
72 dard machine learning methods which rely on balanced classes of data. To mitigate these
73 issues, in this study we explore the potential of a recently developed machine learning
74 method to post-process accumulated precipitation forecasts: a U-Net CNNs architecture
75 (Ronneberger et al., 2015). U-Net CNNs are a form of artificial neural network , which
76 have been used for both classification and regression tasks primarily focused on spatial
77 data in the field of biomedical imaging. As such, this CNN leverages spatial interdepen-
78 dence by construction. Further, we propose and test a dual ML model structure to rec-
79 tify the class imbalance in the sparse precipitation data.

80 In Section 2 we introduce the data used in this study. Section 3 describes the method-
81 ology, including evaluation strategy and skill scores. The results are presented in section
82 4. Conclusions are provided in section 5, where the potential of U-Net CNN as a tool
83 for weather forecasting and future research is discussed.

84 **2 Data and Methodology**

85 **2.1 Observational Data**

86 The observed precipitation data used in this study is the Parameter-elevation Re-
87 lationships on Independent Slopes Model (PRISM) dataset (PRISM Climate Group, 2004),
88 which is constructed using data from the Cooperative Observer Program (COOP) and
89 Snowpack Telemetry (SNOTEL) networks, and a variety of smaller networks (Daly et
90 al., 2008). PRISM provides estimates of accumulated 24 hour precipitation data over the
91 last 40 years over the contiguous United States (CONUS) at a spatial resolution of 4 km.
92 Here we focus on the western United States region comprising California and Nevada.

93 The PRISM dataset was chosen as ground truth in this study due to its accuracy,
94 comparable spatial resolution to the model reforecast data, and length of record. PRISM
95 uses a comprehensive linear precipitation–elevation correction scheme that applies weights
96 based on location to nearby stations, proximity to coast, topographic facets, boundary
97 layer conditions, surrounding terrain height, and other terrain features (Daly et al., 2008).
98 PRISM has been shown to perform well in challenging complex terrain settings when tested
99 against independent station data (Daly et al., 2017). It has also been shown to produce
100 reliably similar estimates of precipitation extremes when compared to other national in-
101 situ based gridded datasets, while performing notably better than various reanalysis prod-
102 ucts (Gibson et al., 2019).

103 **2.2 Model Reforecast Data**

104 The NWP reforecast data which is being post-processed, was developed at the Cen-
105 ter for Western Weather and Water Extremes. As input to the U-Net CNN, we use weather
106 forecasts over a 3-km domain (Figure 1) of 34 water years (1985 to 2019) of the West-
107 ern Weather Research and Forecasting (West-WRF) regional model (Martin et al., 2019)
108 covering the western United States, California and Nevada. The forecasts are driven by

109 initial and boundary conditions from the Global Forecasting System. The West-WRF
110 regional model has shown forecast skill with a low intensity error for IVT and reduced
111 dry and wet biases for precipitation over lead times from 1 to 7 days (see Steinhoff et
112 al. (2020) for additional details on the reforecast).

113 To align the forecast spatially with the observation set, we regrid the forecasts with
114 a nearest-neighbor approach to a 4-km resolution, to retain existing precipitation pat-
115 terns and preserve global precipitation means. For temporal alignment with the obser-
116 vations, and given that the forecast are initialized daily at 0000 UTC, we calculate the
117 accumulated daily precipitation offset by 12 hours to account for model spin-up. In other
118 words, data from 12-h to 36-h after initialization of each West-WRF forecast is labelled
119 as Day 1 forecast and is aligned with PRISM ground truth data.

120 **2.3 Machine Learning Approach**

121 The proposed CNN for forecast post-processing uses the U-Net architecture as a
122 baseline, named after its distinctive U-shape model diagram (Ronneberger et al., 2015).
123 Historically, this type of CNN has been used for biomedical image segmentation, but its
124 application with weather forecasts is promising given its strength in rectifying spatial
125 biases through image segmentation (W. Chapman et al., 2019). The model architecture
126 consists of two phases. In the first phase, the model performs data compression through
127 repeated convolutional layers to learn spatial features. This is followed by an expand-
128 ing phase in which the output image is reconstructed using the learned features. We mod-
129 ified the U-Net architecture as introduced by Ronneberger et al. (2015) in several ways
130 as detailed below to adapt it to the task of improving the skill of precipitation forecasts.
131 The model along with these modifications is referred to as the modified U-Net CNN from
132 here onwards.

133 West-WRF model output variables are used as predictors in the CNN. In partic-
134 ular, to generate Day 1 predictions, the normalized 24-h accumulated precipitation, and
135 the 6, 12 and 18-h forecasts of 5-m specific humidity and 2-m temperature since fore-
136 cast initialization are used. Similarly, for greater lead times, we use the same predictors
137 offset by the lead times. These predictors are used because they provide significant in-
138 sight into the ground truth precipitation (Richardson, 1922). It was determined through
139 validation that as the number of input parameters was increased beyond these predic-
140 tors and time granularity (e.g., hourly instead of 6 hourly), the efficiency and accuracy
141 of the model decreased (Anelli et al., 2019).

142 The loss function used for the modified U-Net CNN is an asymmetric adaptation
143 of the mean-square error that penalizes underprediction more than overprediction. It was
144 observed through preliminary tests that the U-Net CNN tended to systematically un-
145 derpredict extreme precipitation events, hence we chose to correct this bias as follows.
146 We assign a hyperparameter $w_s > 1$ that multiplicatively weights underpredicted val-
147 ues as described in Equation S2 in the supplemental information. The value of w_s is de-
148 termined by minimizing loss on the validation data set, which is consistent with the pro-
149 cedure to determine all hyperparameters.

150 To combat a tendency for neural networks to predict small non-zero values of pre-
151 cipitation for every grid cell due to millions of additions in its numerical computations
152 (for example, a "zero" value might be predicted as 0.001), we leverage binary masking,
153 during model training, for precipitation prediction (Hayatbini et al., 2019). Binary mask-
154 ing is a classification technique that generates a rain vs. no rain map for all grid points
155 given the same input as the main post-processing framework. We use the same model
156 architecture for training this binary mask predictor as the main post-processing model
157 except the predictions (the numerical precipitation value) are replaced by indicator func-
158 tions of the precipitation (i.e., rain vs. no rain). We train this completely separately from
159 the main post-processing model. In other words, instead of predicting the amount of pre-

160 precipitation, we predict the probability of non-zero precipitation at that grid point. Then,
 161 we use masking to remove any values in the main numerical precipitation prediction that
 162 were predicted as likely having zero rain with over 50% probability by our binary mask.
 163 The loss function used in this case is the cross-entropy loss, a standard loss used in this
 164 kind of classification problems (Hayatbini et al., 2019). Figure S1 summarizes the afore-
 165 mentioned structure, located in the supplemental information.

166 Further, we propose a dual ML model solution to class imbalance between the oc-
 167 currence of extreme and moderate precipitation events. We will refer to this as the dual
 168 model approach. For extreme events, traditional machine learning-based baselines such
 169 as MOS tend to underestimate the upper tail of the distribution and overestimate the
 170 moderate case due to the relatively low probability of extreme values in the distribution.
 171 To address this issue, we create separate U-Net CNN models for the more extreme events
 172 as classified by mean forecast accumulated precipitation above 2.5 mm. This corresponds
 173 with roughly all events below the 20th percentile total accumulated precipitation, which
 174 was determined through validation as an effective separation to mitigate the class im-
 175 balance issue. For the remaining events, we train a separate U-Net model to preserve
 176 predictive capability for the moderate case. Through this, we accomplish a tailored model
 177 for both extreme and moderate precipitation. While there exist deep learning techniques
 178 that resolve class imbalances in a more formal way such as data augmentation, they rely
 179 on mutating the data (e.g., stretching or cropping), which may be less desirable for post-
 180 processing problems with a numerical output (Perez & Wang, 2017). This is because these
 181 techniques produce an augmented input, but the numerical output (ground truth) then
 182 needs to be augmented too. Hence, we don't perform this and instead assume that gen-
 183 eral mean and total precipitation over a region is roughly consistent in distribution over
 184 water years.

185 Parameter tuning for the learning rate, the number of filters per layer, and loss func-
 186 tion weights is accomplished through validation. The optimal hyperparameters were close
 187 to their default values as provided in Keras, the used machine learning library (Chollet
 188 et al., 2015). The values and more detailed information regarding hyperparameter tun-
 189 ing are provided in the supplementary information.

190 2.4 Testing and Evaluation

191 The CNN is evaluated over a chosen test set of 4 water years, which were selected
 192 based on categorical El Niño/Southern Oscillation years. We use one El Niño year (1997),
 193 one La Niña year (2011), and two ENSO neutral years: one historically wet and one dry
 194 year (years 2016 and 2013, respectively). ENSO years have been shown to dramatically
 195 effect West Coast precipitation regimes through large scale pressure patterns which sig-
 196 nificantly alter precipitation predictability (W. E. Chapman et al., 2021; Kumar & Ho-
 197 erling, 1998). We also select particularly wet (2016/2017) and dry (2013/2014) years in
 198 which ENSO is in a neutral state, representing California drought conditions and a sur-
 199 plus of precipitation, respectively, without tropical SST forcing. We choose these years
 200 in order to test the skill of our methods in varied climate regimes and on a variety of pre-
 201 cipitation events. The rest serves as the training set. We use a testing process that most
 202 closely mimics a production system in which we train one CNN model over all possible
 203 years except a singular testing year and a validation year (the latter used to tune the
 204 hyperparameters); this is done for all years, so we train 4 dual ML models in total (8 in
 205 total), each of which is not trained on their corresponding test year. We refer to this as
 206 "one-shot" training.

207 Traditional machine learning and dynamical post-processing frameworks were com-
 208 pared to the proposed U-Net CNN to assure its predictive accuracy and reliability over
 209 the chosen test set. Further, they offered a baseline for the CNN's forecasting skill. A
 210 prediction based on climatology was used to ensure that the CNN is consistent and re-

211 liable. It was constructed by averaging 30 days worth of observation data prior to any
 212 particular testing day over all years preceding it. The second comparison was with the
 213 West-WRF dynamical model, which is used as the input to the machine learning method.
 214 As such, any rectification of spatial or temporal biases over the West-WRF model would
 215 be directly reflected in the CNN’s accuracy and errors. Further, we implemented a MOS
 216 based on a L1-regularized multilinear regression (Tibshirani, 1996). The MOS presents
 217 a more traditional ML framework that can be used as a baseline to the CNN. Similar
 218 to many other ML frameworks, the MOS leverages point-based learning as opposed to
 219 the strategy adopted in a CNN. Note that the multilinear regression is configured to use
 220 the same predictors (precipitation, humidity, temperature) as the CNN and uses the same
 221 “one-shot” training for consistency.

222 We evaluated the model using the following metrics: root-mean square error (RMSE),
 223 mean absolute error (MAE), model BIAS (BIAS), critical success index (CSI), and Pear-
 224 son correlation (PC). These metrics provide a comprehensive aggregated point-by-point
 225 analysis of the CNN’s performance with regards to the numerical error and the categor-
 226 ical accuracy. The mathematical equations for each are shown in Equation S3.

227 Similarly to Sperati et al. (2017), to verify the spatial consistency of the predic-
 228 tion generated by each of the methods, we also compare the pairwise correlation between
 229 all pairs of grid points for the predictions with the observations. When the pairwise cor-
 230 relation between a chosen model’s grid points (e.g., the CNN) more closely matches the
 231 pairwise correlation for the ground truth grid points, it indicates a greater degree of cor-
 232 respondence in terms of spatial relationships in the ground truth.

233 3 Results

234 The U-Net CNN post-processed forecasts are compared against several methods.
 235 Figure 1 shows an example of a 96 h forecast of an extreme event that occurred on Febru-
 236 ary 10, 2014 in the test set. The multilinear regression post-processing and West-WRF
 237 model overpredict over the highlighted heavy precipitation areas. Comparatively, the CNN
 238 qualitatively more closely resembles the observation patterns of the event as estimated
 239 by PRISM, especially within the heavy precipitation regions. For this case, it produces
 240 the lowest RMSE with respect to the PRISM ground-truth field, improving upon West-
 241 WRF by 33.9% and MOS by 8.1%. This is an example of CNN’s ability to correct for
 242 spatial biases in the forecasts.

243 3.1 Discussion of Evaluation Metrics

244 The models are compared with respect to all the error metrics defined in Section
 245 2.4: RMSE, MAE, PC, and CSI. All of the shown metrics and improvements were boot-
 246 strap sampled and produced with a 95% confidence interval to indicate if the results are
 247 statistically significant.

248 The CNN’s overall RMSE aggregated over the 4 lead times (1-4 days) consistently
 249 outperformed climatology by 34.1-37.0%, West-WRF by 12.9-15.9%, and MOS by 7.4-
 250 8.9%. Similarly, the CNN outperformed both West-WRF and MOS for all 4 lead times
 251 with respect to Pearson correlation (PC) by 2.7-3.4% and 3.3-4.2%, respectively. Over
 252 the same period, the CNN improved upon West-WRF’s CSI by 0.6-1.5%, with greater
 253 improvements ranging from 2.7% to 5.6% for lead times of 24 to 48 h. Note that we do
 254 not provide a complete set of improvement statistics for CLIM apart from RMSE since
 255 it is consistently 40-50% improved upon with regard to every metric.

256 Further, we analyze the performance of the models on the top 10% most heavy pre-
 257 cipitation events. The CNN’s overall RMSE/MAE over these events was reduced 19.8-
 258 21.0/17.7-18.3% and 8.8-9.7/5.4-6.2% compared to West-WRF and MOS respectively

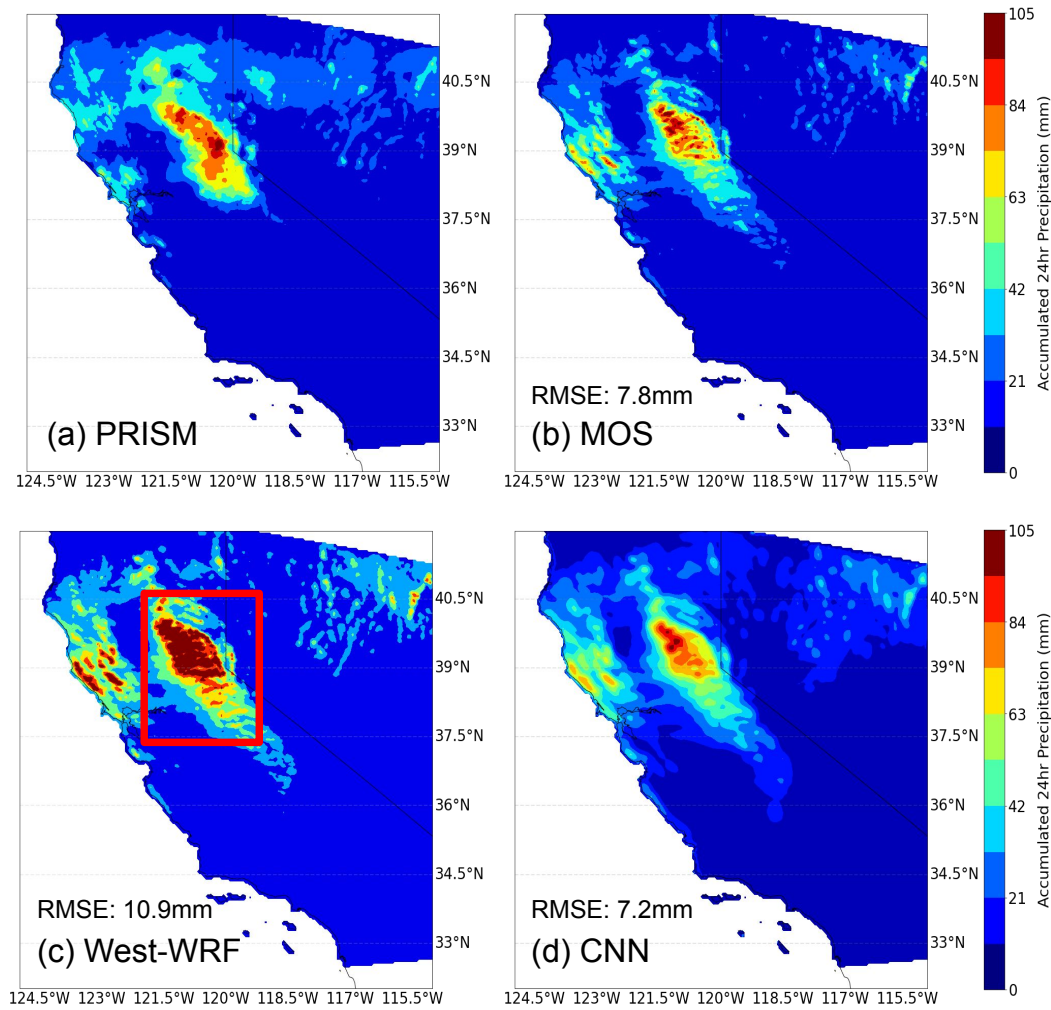


Figure 1. The 24-h accumulated precipitation on February 10, 2014 (test set) for (a) PRISM, (b) MOS, (c) West-WRF, and (d) CNN. The RMSE for each method with respect to the PRISM observation (a) is (b) 7.8 mm, (c) 10.9 mm, and (d) 7.2 mm. The highlighted region in red showcases an area of strong overprediction in West-WRF.

259 over all lead times of 1-4 days. Further, the CNN's PC over these events was improved
 260 by 4.9-5.5% and 4.2-4.7% compared to West-WRF and MOS.

261 Since the latter two metrics, PC and CSI, showcase the spatial and categorical ac-
 262 curacy of the methods, and RMSE summarizes the numerical accuracy, the CNN clearly
 263 outperformed the other post-processing and dynamical methods over all lead times with
 264 respect to spatial, categorical, and numerical accuracy aggregated over heavy precipi-
 265 tation and all events. These improvements are all shown to be statistically significant
 266 over a 95% confidence interval. The complete comparison for each error metric over each
 267 model is included in the supplemental information for all lead times.

268 These improvements are qualitatively consistent or better over similar dynamical
 269 baselines as cited in recent literature regarding machine learning-based post-processing
 270 methods. In Roulin and Vannitsem (2012), probabilistic techniques such as logistic re-
 271 gression are used to improve precipitation forecasts. Over the forecasting period, the MSE
 272 throughout the forecasting period is 5-15% better than the baseline dynamical method,

273 which is consistent with the multilinear regression model presented in this study that
 274 is shown to be 28-31% inferior to the CNN in terms of MSE.

275 3.2 Temporal Evaluation of Models

276 We show some of the error metrics (RMSE, CRMSE, BIAS, PC) for each post-processing
 277 and dynamical method as a function of the lead time in Figure 2. This allows a more
 278 thorough examination of the propagation of error through increasing lead times.

279 Specifically, the RMSE is decomposed into bias, which reflect systematic errors, and
 280 CRMSE, which includes random errors and conditional biases, as indicated in Equation
 281 S1. Throughout the 4 lead times, the CNN consistently has the lowest CRMSE, as well
 282 as the highest Pearson correlation. In fact, the CNN is consistently able to add a day
 283 worth of predictive skill when compared to West-WRF (i.e. CNN error on day 4 is less
 284 than West-WRF error on day 3) in terms of RMSE, CRMSE, and PC. The BIAS fluctu-
 285 ates for each post-processing and forecasting method, but it is significantly lower than
 286 the CRMSE and contributes only marginally to the RMSE. This means that the CNN
 287 is able to improve the predictive ability of the dynamical model while minimally increas-
 288 ing the systematic errors (when compared to total RMSE).

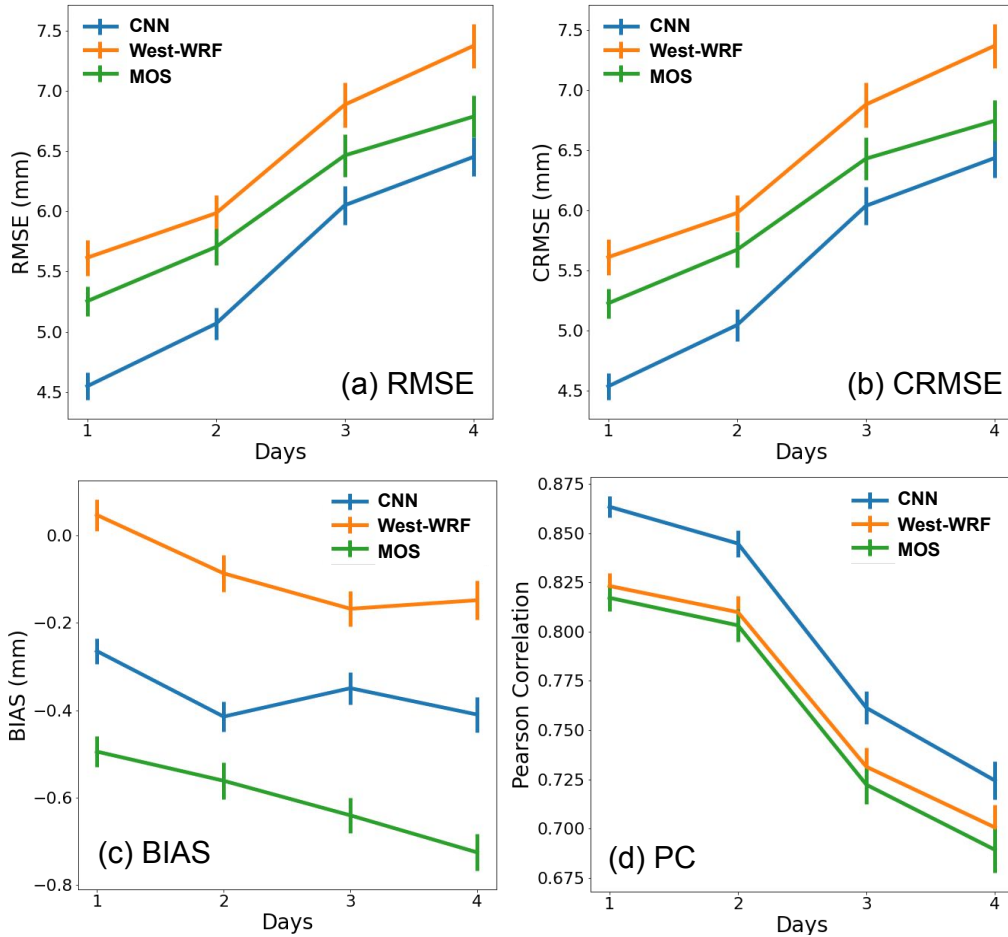


Figure 2. Pearson's correlation, CRMSE, RMSE, and BIAS for each model as a function of model lead time in days.

Further, we evaluate the rate of growth of the error metrics to evaluate the CNN’s capabilities of producing longer-term forecasts and the scaling of the error as a function of lead time. A slower rate of growth of all error metrics would indicate a method that tracks better as a function of lead time. The average rate of growth for RMSE is significantly higher for West-WRF between days 2-4 as compared to CNN, with a reduction of 17.9% from day 3 to 4. Similarly, the average rate of decay for PC is reduced by 16.6% for the CNN as compared to West-WRF over days 2-4. Effectively, the CNN add more than one day of predictive skills to West-WRF, as for example is indicated by the CNN’s RMSE at day 4, which is between the RMSE of West-WRF at days 2 and 3.

3.3 Spatial Evaluation of Models

The spatial patterns of improvement in error metrics as compared to West-WRF, aggregated over lead times of Day 1 to Day 4, is shown in Figure 3. The improvement in RMSE and MAE are consistently above 10%, with significant improvements of around 30-40% in the Sierra Nevada region. Similarly, the CNN improves upon West-WRF’s Pearson correlation coefficient 5% or more, with significant improvements of 10-15% in southern California. The sharp decrease in correlation in the northern region and throughout the California Channel Islands is likely attributed to the CNN’s documented weaknesses to domain boundaries due to spatial padding for convolution (Alsallakh et al., 2020). The CNN’s improvements in CSI are largely mixed, with coastal California showing around 10% improvement over West-WRF. In southern California and Nevada, the West-WRF model outperforms the CNN by 15%. However, it is important to note that regions in which the CNN more significantly underperforms (the highlighted blue regions) account for only 9.2% of the total precipitation in the region (i.e., they are dry areas).

The spatial consistency of the generated precipitation field is also examined using a pairwise correlation plot (Sperati et al., 2017). This is an important aspect of the forecast evaluation because it explores the ability of the CNN to capture the spatial distribution of observed precipitation.

The pairwise correlation plot is shown in Figure 4 for both the CNN and West-WRF methods. With a perfect forecasting or post-processing method, we expect the correlation between each of the grid cells to match with the observation set, as shown by the 1:1 line in orange. The actual distribution of pairwise correlations between the CNN and West-WRF with respect to the PRISM is shown as a density plot. Qualitatively, it is noted that the CNN maintains the spatial attributes of the PRISM observations just as well as West-WRF by the fact that the spread is just as concentrated along 1:1 line. The higher coefficient of determination (R^2) of the CNN pairwise correlation plot indicates that the dispersion around the identity is lower than that of the West-WRF pairwise correlation plot. This indicates the CNN’s superior spatial consistency with the PRISM ground truth as compared to West-WRF. Note that this analysis does not factor in the observational error.

4 Conclusions

The U-Net Convolutional Neural Network (CNN) architecture originally proposed by Ronneberger et al. (2015) and adapted in this study for precipitation prediction provides a computationally efficient and consistently accurate post-processing framework over different types of water years that outperforms competing machine learning and dynamical models. It provides superior spatial consistency and numerical accuracy over all lead times as summarized by the 12.9-15.9% improvement in root-mean-square error (RMSE) over the Western Weather Research and Forecasting model and 7.4-8.9% improvement over Model Output Statistics. It also displays a reduce rate of error growth such as RMSE and Pearson’s correlation as lead times increase, which effectively results in more than a day of additional predictive skill with respect to a dynamical model. Ad-

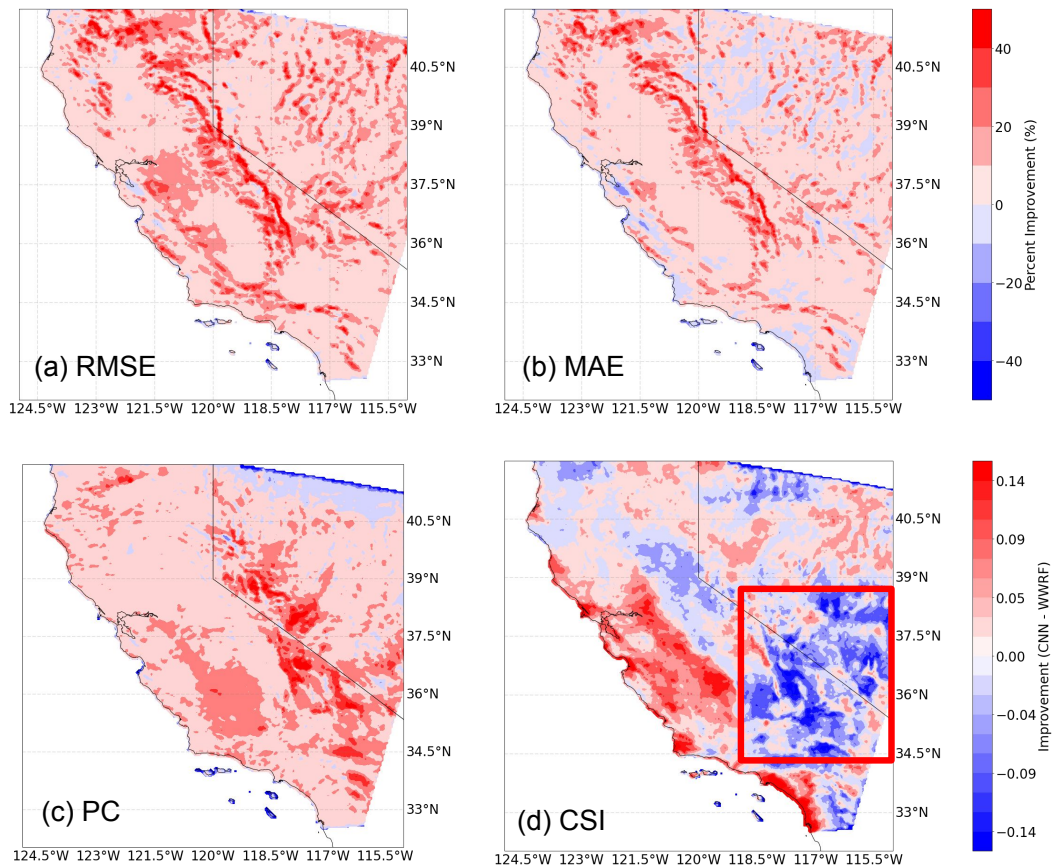


Figure 3. The CNN's improvement/degradation in RMSE, MAE, PC and CSI as compared to the West-WRF regional model aggregated over all lead times (1-4 days). Highlighted region shows an area of severe reduction in CSI for the CNN, see discussion in text.

339 Additionally, the CNN outperforms the other methods for the prediction of the top 10%
 340 precipitation events. This demonstrates a consistent and reliable post-processing frame-
 341 work that improves upon spatial and temporal biases over dynamical models and other
 342 post-processing methods over the western US. Future work includes examining the tem-
 343 poral association between day-to-day forecasts using recurrent neural networks or trans-
 344 formers along with an encoding convolutional neural network. The Convolutional Long
 345 Short-Term Memory layer developed by Shi et al. (2015) provides a promising avenue
 346 to explore this further. Additional methods to rectify the class imbalance can be explored,
 347 such as data augmentation.

348 Acknowledgments

349 This research was supported by USACE FIRO grant W912HZ1520019 and CDWR AR
 350 Program grant 4600013361.

351 References

352 Alessandrini, S., Delle Monache, L., Sperati, S., & Nissen, J. (2015). A novel appli-
 353 cation of an analog ensemble for short-term wind power forecasting. *Renewable*
 354 *Energy*, *76*, 768-781. Retrieved from <https://www.sciencedirect.com/science/article/pii/S0960148114007915> doi: <https://doi.org/10.1016/>

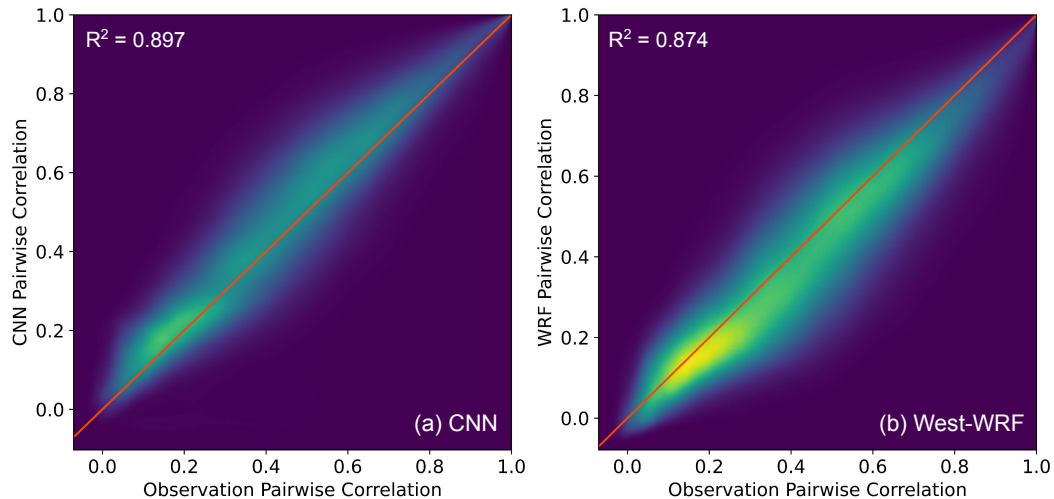
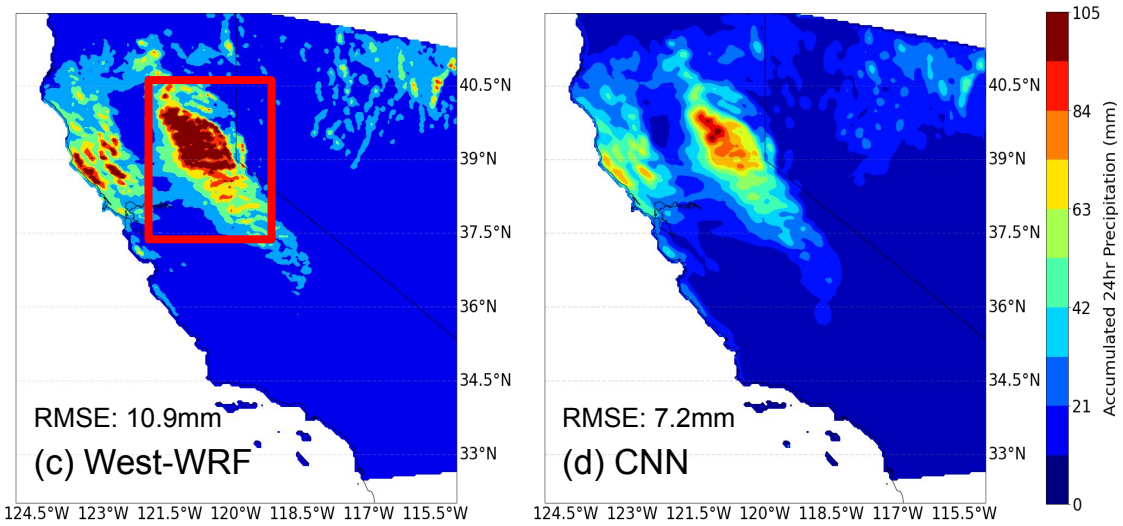
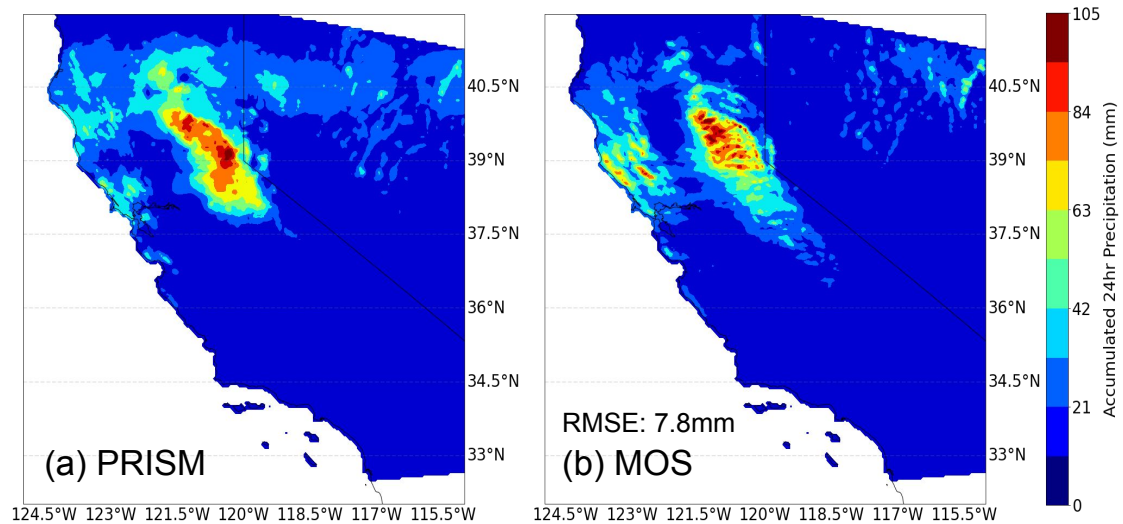


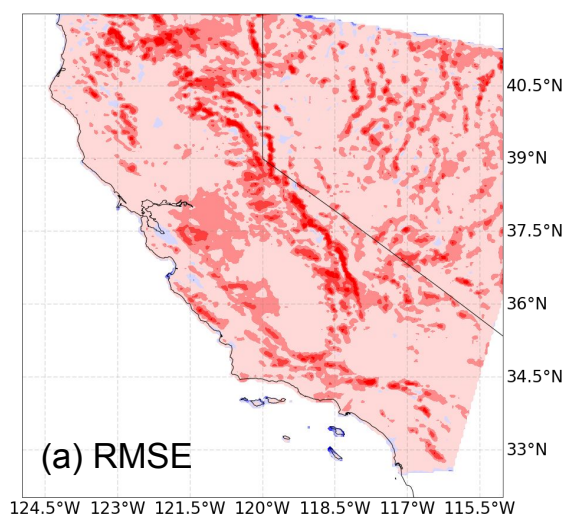
Figure 4. The CNN’s (left) and West-WRF (right) pairwise correlation plot with the PRISM observations. The coefficient of determination (R^2) is shown in the upper left of both panels. The orange line denotes a perfect correspondence in observation and model pairwise correlation between grid points.

- 356 j.renene.2014.11.061
 357 Alsallakh, B., Kokhlikyan, N., Miglani, V., Yuan, J., & Reblitz-Richardson,
 358 O. (2020). Mind the pad—cnns can develop blind spots. *arXiv preprint*
 359 *arXiv:2010.02178*.
 360 AMS. (2019). *Glossary of meteorology*. (Retrieved from [http://glossary.ametsoc](http://glossary.ametsoc.org/wiki/atmospheric_river)
 361 [.org/wiki/atmospheric_river](http://glossary.ametsoc.org/wiki/atmospheric_river) at Jun 9, 2021 2:39 PM)
 362 Anelli, V. W., Di Noia, T., Di Sciascio, E., Pomo, C., & Ragone, A. (2019). On
 363 the discriminative power of hyper-parameters in cross-validation and how to
 364 choose them. In *Proceedings of the 13th acm conference on recommender*
 365 *systems* (pp. 447–451).
 366 Cervone, G., Clemente-Harding, L., Alessandrini, S., & Delle Monache, L. (2017).
 367 Short-term photovoltaic power forecasting using artificial neural net-
 368 works and an analog ensemble. *Renewable Energy*, *108*, 274–286. Re-
 369 trieved from [https://www.sciencedirect.com/science/article/pii/](https://www.sciencedirect.com/science/article/pii/S0960148117301386)
 370 [S0960148117301386](https://www.sciencedirect.com/science/article/pii/S0960148117301386) doi: <https://doi.org/10.1016/j.renene.2017.02.052>
 371 Chapman, W., Subramanian, A., Delle Monache, L., Xie, S., & Ralph, F. (2019).
 372 Improving atmospheric river forecasts with machine learning. *Geophysical*
 373 *Research Letters*, *46*(17–18), 10627–10635.
 374 Chapman, W. E., Subramanian, A. C., Xie, S.-P., Sierks, M. D., Ralph, F. M., &
 375 Kamae, Y. (2021). Monthly modulations of enso teleconnections: Implications
 376 for potential predictability in north america. *Journal of Climate*, 1–71.
 377 Chollet, F., et al. (2015). *Keras*. <https://github.com/fchollet/keras>. GitHub.
 378 Collins, M., & Allen, M. R. (2002). Assessing the relative roles of initial and bound-
 379 ary conditions in interannual to decadal climate predictability. *Journal of Cli-*
 380 *mate*, *15*(21), 3104–3109.
 381 Corringham, T. W., Ralph, F. M., Gershunov, A., Cayan, D. R., & Talbot, C. A.
 382 (2019). Atmospheric rivers drive flood damages in the western united states.
 383 *Science advances*, *5*(12), eaax4631.
 384 Daly, C., Halbleib, M., Smith, J. I., Gibson, W. P., Doggett, M. K., Taylor, G. H.,
 385 ... Pasteris, P. P. (2008). Physiographically sensitive mapping of climatolo-
 386 gical temperature and precipitation across the conterminous united states.

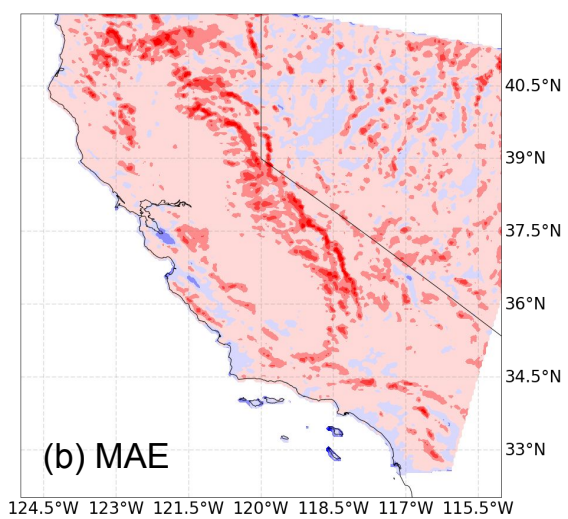
- 387 *International Journal of Climatology: a Journal of the Royal Meteorological*
388 *Society*, 28(15), 2031–2064.
- 389 Daly, C., Slater, M. E., Roberti, J. A., Laseter, S. H., & Swift Jr, L. W. (2017).
390 High-resolution precipitation mapping in a mountainous watershed: ground
391 truth for evaluating uncertainty in a national precipitation dataset. *Internation-*
392 *ational Journal of Climatology*, 37, 124–137.
- 393 Delle Monache, L., Eckel, F. A., Rife, D. L., Nagarajan, B., & Searight, K. (2013).
394 Probabilistic weather prediction with an analog ensemble. *Monthly Weather*
395 *Review*, 141(10), 3498–3516.
- 396 Gibson, P. B., Waliser, D. E., Lee, H., Tian, B., & Massoud, E. (2019). Climate
397 model evaluation in the presence of observational uncertainty: Precipitation
398 indices over the contiguous united states. *Journal of Hydrometeorology*, 20(7),
399 1339–1357.
- 400 Glahn, H. R., & Lowry, D. A. (1972). The use of model output statistics (mos) in
401 objective weather forecasting. *Journal of Applied Meteorology and Climatology*,
402 11(8), 1203–1211.
- 403 Hayatbini, N., Kong, B., Hsu, K.-l., Nguyen, P., Sorooshian, S., Stephens, G., ...
404 Ganguly, S. (2019). Conditional generative adversarial networks (cgans) for
405 near real-time precipitation estimation from multispectral goes-16 satellite
406 imageries—persiann-cgan. *Remote Sensing*, 11(19), 2193.
- 407 Krizhevsky, A., Sutskever, I., & Hinton, G. E. (2012). Imagenet classification with
408 deep convolutional neural networks. *Advances in neural information processing*
409 *systems*, 25, 1097–1105.
- 410 Kumar, A., & Hoerling, M. P. (1998). Annual cycle of pacific–north american
411 seasonal predictability associated with different phases of enso. *Journal of*
412 *Climate*, 11(12), 3295–3308.
- 413 Louka, P., Galanis, G., Siebert, N., Kariniotakis, G., Katsafados, P., Pytharoulis, I.,
414 & Kallos, G. (2008). Improvements in wind speed forecasts for wind power
415 prediction purposes using kalman filtering. *Journal of Wind Engineering and*
416 *Industrial Aerodynamics*, 96(12), 2348–2362.
- 417 Martin, A. C., Ralph, F. M., Wilson, A., DeHaan, L., & Kawzenuk, B. (2019).
418 Rapid cyclogenesis from a mesoscale frontal wave on an atmospheric river:
419 Impacts on forecast skill and predictability during atmospheric river landfall.
420 *Journal of Hydrometeorology*, 20(9), 1779–1794.
- 421 Nicolis, C., & Nicolis, S. C. (2007). Return time statistics of extreme events in deter-
422 ministic dynamical systems. *EPL (Europhysics Letters)*, 80(4), 40003.
- 423 ODonnell, A., Hubbard, T., Nadeau, L., Delaney, C., Hartman, R., Mendoza, J., ...
424 Corringham, T. (2020). Estimating benefits of forecast-informed reservoir
425 operations (firo): Lake mendocino case-study and transferable decision support
426 tool. In *Agu fall meeting 2020*.
- 427 Perez, L., & Wang, J. (2017). The effectiveness of data augmentation in image clas-
428 sification using deep learning. *arXiv preprint arXiv:1712.04621*.
- 429 PRISM Climate Group, O. S. U. (2004). *Prism data*. (Retrieved from [http://prism](http://prism.oregonstate.edu)
430 [.oregonstate.edu](http://prism.oregonstate.edu))
- 431 Ralph, F. M., Rutz, J. J., Cordeira, J. M., Dettinger, M., Anderson, M., Reynolds,
432 D., ... Smallcomb, C. (2019). A scale to characterize the strength and impacts
433 of atmospheric rivers. *Bulletin of the American Meteorological Society*, 100(2),
434 269–289.
- 435 Rasp, S., & Lerch, S. (2018). Neural networks for postprocessing ensemble weather
436 forecasts. *Monthly Weather Review*, 146(11), 3885–3900.
- 437 Richardson, L. F. (1922). *Weather prediction by numerical process*. Cambridge uni-
438 versity press.
- 439 Ronneberger, O., Fischer, P., & Brox, T. (2015). U-net: Convolutional networks for
440 biomedical image segmentation. In *International conference on medical image*
441 *computing and computer-assisted intervention* (pp. 234–241).

- 442 Roulin, E., & Vannitsem, S. (2012). Postprocessing of ensemble precipitation predic-
443 tions with extended logistic regression based on hindcasts. *Monthly weather re-*
444 *view*, *140*(3), 874–888.
- 445 Shi, X., Chen, Z., Wang, H., Yeung, D.-Y., Wong, W.-K., & Woo, W.-c. (2015).
446 Convolutional lstm network: A machine learning approach for precipitation
447 nowcasting. *arXiv preprint arXiv:1506.04214*.
- 448 Sperati, S., Alessandrini, S., & Delle Monache, L. (2017). Gridded probabilistic
449 weather forecasts with an analog ensemble. *Quarterly Journal of the Royal Me-*
450 *teorological Society*, *143*(708), 2874–2885.
- 451 Steinhoff, D., Kawzenuk, B., Weihs, R., Reynolds, D., DeHaan, L., Martin, A., &
452 Delle Monache, L. (2020). Nrt wy2020 post-season report.
- 453 Tao, Y., Gao, X., Hsu, K., Sorooshian, S., & Ihler, A. (2016). A deep neural net-
454 work modeling framework to reduce bias in satellite precipitation products.
455 *Journal of Hydrometeorology*, *17*(3), 931 - 945. Retrieved from [https://](https://journals.ametsoc.org/view/journals/hydr/17/3/jhm-d-15-0075_1.xml)
456 journals.ametsoc.org/view/journals/hydr/17/3/jhm-d-15-0075_1.xml
457 doi: 10.1175/JHM-D-15-0075.1
- 458 Tibshirani, R. (1996). Regression shrinkage and selection via the lasso. *Journal of*
459 *the Royal Statistical Society: Series B (Methodological)*, *58*(1), 267–288.
- 460 Vannitsem, S., & Ghil, M. (2017). Evidence of coupling in ocean-atmosphere dynam-
461 ics over the north atlantic. *Geophysical Research Letters*, *44*(4), 2016–2026.

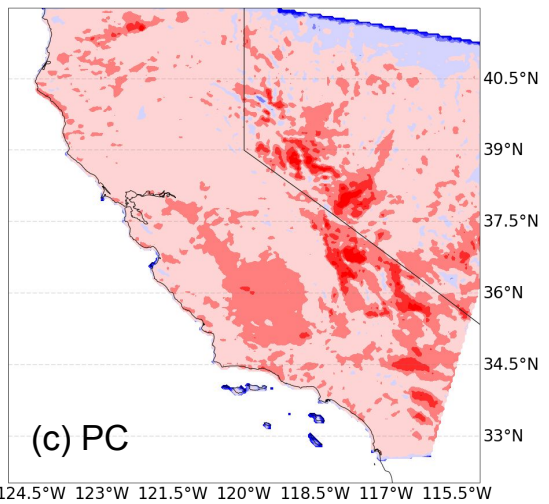
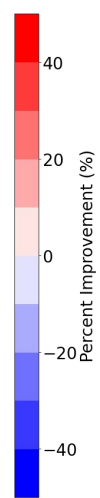




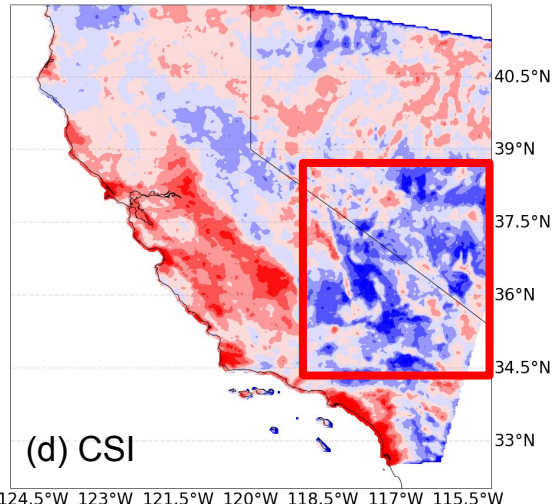
124.5°W 123°W 121.5°W 120°W 118.5°W 117°W 115.5°W



124.5°W 123°W 121.5°W 120°W 118.5°W 117°W 115.5°W



124.5°W 123°W 121.5°W 120°W 118.5°W 117°W 115.5°W



124.5°W 123°W 121.5°W 120°W 118.5°W 117°W 115.5°W

